Ultrasonic Beam Field Modeling - Fundamentals and Applications in Nondestructive Evaluation

Martin Spies
Fraunhofer-Institute Zerstörungsfreie Prüfverfahren (IZFP)
University of Saarland, Bldg. 37, 66123 Saarbrücken, Germany

Abstract

To ensure the reliability of ultrasonic nondestructive evaluation techniques for modern structural materials, the effects of anisotropy and inhomogeneity and the influence of nonplanar component geometries on ultrasonic wave propagation have to be taken into account. In this contribution, fundamentals and applications of two analytical approaches to three-dimensional elastic beam field calculation are presented. Results for both isotropic materials including curved interfaces and for anisotropic media like composites and weld material are presented, covering field profiles for various types of transducers and the modeling of time-dependent rf-signals.

Introduction

In ultrasonic nondestructive evaluation use is made of the physical properties of elastic waves in solids in order to detect defects and material inhomogeneities. To ensure the reliability of ultrasonic inspection techniques for modern structural materials, the effects of anisotropy and inhomogeneity and the effects of non-planar component geometries on ultrasonic wave propagation have to be taken into account. In this contribution, fundamentals and applications of two analytical approaches to three-dimensional elastic wavefield calculation are presented, which can applied to model ultrasound generation, propagation and scattering in complex-structured materials and components.

Based on a mathematical formulation involving Green's dyadic displacement tensor function, appropriate evaluation yields a representation of the displacement vector of transducer wavefields which is convenient for effective numerical computation. With respect to bulk wave propagation the numerical evaluation of Green's dyadic function - which is particularly tedious in the anisotropic case - is circumvented by applying a reciprocity-based approach, valid in the (point source) far-field. The presented formulation involves characteristic quantities obtained from plane wave theory and appears as a point source superposition representation including the respective point source directivities. The approach allows to include all aspects relevant to testing simulation for such configurations as far as bulk wave propagation is concerned [1,2].

Among a variety of methods for transducer field calculation, beam superposition has proven to be highly efficient for circular single-element apertures. A Gaussian beam approach for anisotropic media will be presented, where each of the Gaussian base functions is furnished with coefficients fixing the beam waists and their position. The method is especially suited for beam field calculations in inhomogeneous media [3,4].

Representative results for both isotropic materials including curved interfaces and for anisotropic media like composites and weld material are presented, covering field profiles for various types of transducers and the modeling of time-dependent rf-signals. Simulation-assisted transducer optimization is also illustrated for both single-element and multiple-element probes.

Fundamentals

Equation of Motion

The dynamic behaviour of a linear elastic medium can be described by the equation of motion for the displacement vector $\underline{\mathbf{u}}$. For a homogeneous solid it can be written in a general form according to

$$(\underline{\nabla} \cdot \underline{\underline{\underline{\underline{\mathbf{C}}}}} \cdot \underline{\nabla}) \cdot \underline{\mathbf{u}} + \varrho\omega^2 \underline{\mathbf{u}} = -\,\underline{\mathbf{f}}\,, \qquad (1)$$

where ϱ is the mass density, $\underline{\nabla}$ is the gradient vector, $\underline{\mathbf{f}}$ accounts for the volume force density and ω denotes the circular frequency, if a time dependence $\sim \mathrm{e}^{-\mathrm{j}\omega\mathrm{t}}$ is assumed. The elastic properties of the homogeneous solid are described by the fourth rank elastic (stiffness) tensor, which depends on the elastic material constants. A most general representation for this tensor has been given recently for orthotropic media of arbitrary orientation [2], which includes the higher symmetries tetragonal, transversely isotropic, cubic and isotropic as special cases.

Plane Waves

The plane wave solutions are in the form

$$\underline{\mathbf{u}}_\alpha(\underline{\mathbf{R}},\omega) = U\,\underline{\hat{\mathbf{u}}}_\alpha \exp\left[\mathrm{j}\,K_\alpha \underline{\hat{\mathbf{K}}}\cdot\underline{\mathbf{R}}\right], \qquad (2)$$

where $\underline{\hat{\mathbf{K}}}$ is the propagation direction, U is the (complex) amplitude and α denotes the wave type. The determination of the polarization vectors $\underline{\hat{\mathbf{u}}}_\alpha$ and the wave numbers K_α can be performed by applying Fourier-transforms with respect to $\underline{\mathbf{R}}$ in terms of

$$\tilde{\underline{\mathbf{u}}}(\underline{\mathbf{K}},\omega) \;=\; \int_{-\infty}^{\infty} \underline{\mathbf{u}}(\underline{\mathbf{R}},\omega)\;\mathrm{e}^{-\mathrm{j}\underline{\mathbf{K}}\cdot\underline{\mathbf{R}}}\;\mathrm{d}^3\underline{\mathbf{R}} \quad (3)$$

to the equation of motion (1) for $\underline{\mathbf{f}} = \underline{\mathbf{0}}$. This yields the dispersion equation

$$\underline{\underline{\tilde{\mathbf{W}}}}(\underline{\mathbf{K}},\omega)\cdot\tilde{\underline{\mathbf{u}}}(\underline{\mathbf{K}},\omega) = \underline{\mathbf{0}}\;, \qquad (4)$$

where the tilde denotes the transformed quantities. In this equation, the 3d-space-time-Fourier representation of $\underline{\mathbf{u}}$ appears as well as the wave matrix

$$\underline{\underline{\tilde{\mathbf{W}}}}(\underline{\mathbf{K}},\omega) = \underline{\mathbf{K}}\cdot\underline{\underline{\underline{\mathbf{C}}}}\cdot\underline{\mathbf{K}} - \varrho\omega^2\,\underline{\underline{\mathbf{I}}}\;, \qquad (5)$$

where $\underline{\underline{\mathbf{I}}}$ is the unity matrix. The polarization vectors $\underline{\hat{\mathbf{u}}}_\alpha$ and the wave numbers K_α can be obtained as the eigenvectors and the eigenvalues of the wave matrix. The latter provide the modulus of phase velocity v_α according to $v_\alpha = \mid \underline{\mathbf{s}}_\alpha \mid^{-1}$ with slowness $\underline{\mathbf{s}}_\alpha = K_\alpha\underline{\hat{\mathbf{K}}}\,/\omega$.

In anisotropic media, the phase velocity is different from the velocity of energy transport, which is in the case of lossless materials given by the group velocity according to

$$\underline{\mathbf{c}}_\alpha = \left(v\,\frac{\partial K}{\partial\underline{\mathbf{K}}} + K\,\frac{\partial v}{\partial\underline{\mathbf{K}}}\right)_{\underline{\mathbf{K}}_\alpha} \qquad (6)$$

For transversely isotropic and orthotropic materials with arbitrary spatial orientation, these quantities have been given previously [1,2].

Bulk Wave Properties

In an isotropic medium, one can distinguish between the compressional (P) and the horizontally or vertically polarized shear waves (SH and SV). The decomposition into these three eigenwaves is based on the orientation of the polarization vectors with respect to the horizontal plane. In a weakly anisotropic medium, the plane waves can still be labeled as quasi-P (qP), with approximately longitudinal polarization, and quasi-SH (qSH) and quasi-SV (qSV), with approximately transverse polarization. In a strongly anisotropic medium, there are three plane waves with mutually orthogonal polarizations in every direction of propagation. These are designated as qP, $qS1$ and $qS2$ according to their polarizations when propagated in certain symmetry directions. The speeds of these waves are different and vary with direction. Additionally, the directions of phase flow and energy flow involved with these waves are different, so that phase and group velocity have to be discerned.

Consideration of Multilayered Media

Each interface between the layers produces reflected and refracted waves, which is considered by evaluating the respective conditions of continuity. For planar interfaces, Cartesian coordinates with unit vectors $\{\underline{\mathbf{e}}_x,\ \underline{\mathbf{e}}_y,\ \underline{\mathbf{e}}_z\}$ can be used, so that the interface lies in the x-y-plane. Assuming ideal rigid contact between adjacent layers requires the continuity of the slownesses ($\underline{\mathbf{s}}\cdot\underline{\mathbf{e}}_i$ continuous, $i = x, y$, 'Snell's law') and the continuity of the particle displacements and the normal tractions according to

$$U^I\underline{\mathbf{u}}^I + \sum_\alpha U^{R\alpha}\underline{\mathbf{u}}^{R\alpha} \;=\; \sum_\alpha U^{T\alpha}\underline{\mathbf{u}}^{T\alpha}, \quad (7)$$

$$\underline{\mathbf{e}}_z\cdot\underline{\underline{\mathbf{T}}}^I + \sum_\alpha \underline{\mathbf{e}}_z\cdot\underline{\underline{\mathbf{T}}}^{R\alpha} \;=\; \sum_\alpha \underline{\mathbf{e}}_z\cdot\underline{\underline{\mathbf{T}}}^{T\alpha}, \quad (8)$$

where $\underline{\underline{\mathbf{T}}}$ designates the stress tensor. From these equations, the amplitudes $U^{R\alpha}$ and $U^{T\alpha}$ of the reflected and transmitted waves of type α can be determined in dependence of the incident amplitude U^I. In the case of non-planar interfaces, these boundary conditions have to be applied locally.

The local structure of an inhomogeneous medium can be described by dividing it into several layers, each of them having different elastic properties. In the case of continuously varying elastic material properties a large number of such fictitious layers has to be introduced, while in the case of layered media the original structure can be incorporated into the applied model as it is.

Analytical Modeling Approaches

Point Source Superposition

The basis for the elastodynamic beam field calculation procedure presented here is the mathematical formulation of Huygens' principle given by Pao and Varatharajulu [5]. For wave radiation by an isolated vibrating body or a fixed surface enclosing a source, where each point on the surface S of the body vibrates with the same angular frequency ω, the displacement vector outside the surface S can be written as

$$\underline{\mathbf{u}}(\underline{\mathbf{R}},\omega) = \int\int_S \Big\{\underline{\mathbf{u}}(\underline{\mathbf{R}}',\omega)\cdot\Big[\underline{\mathbf{n}}\cdot\underline{\underline{\boldsymbol{\Sigma}}}(\Delta\underline{\mathbf{R}},\omega)\Big] - \Big[\underline{\mathbf{n}}\cdot\underline{\underline{\mathbf{T}}}(\underline{\mathbf{R}}',\omega)\Big]\cdot\underline{\underline{\mathbf{G}}}(\Delta\underline{\mathbf{R}},\omega)\Big\}\,\mathrm{d}S', \qquad (9)$$

where - with $\underline{\underline{\mathbf{T}}}$ being the stress tensor - the traction $\underline{\mathbf{n}}\cdot\underline{\underline{\mathbf{T}}}$ and the displacement $\underline{\mathbf{u}}$ at this surface act as sources of the generated wavefield. With $\Delta\underline{\mathbf{R}} \equiv (\underline{\mathbf{R}} - \underline{\mathbf{R}}')$, $\underline{\underline{\mathbf{G}}}$ and $\underline{\underline{\boldsymbol{\Sigma}}}$ are Green's dyadic and triadic functions, whose components represent the displacement and stress field, respectively, at position $\underline{\mathbf{R}}$ generated by three mutually perpendicular (point) forces acting at $\underline{\mathbf{R}}'$ on surface S.

For evaluating transducer radiation, S is assumed to lie in the x-y-plane of a Cartesian coordinate system, i.e. $\underline{\mathbf{n}} = \underline{\mathbf{e}}_z$. In selecting the Green's tensor functions entering in Eq. (9) one has two options. The first one is to choose the free-space functions as has been done e.g. by Guo and Achenbach [6], where, however, $\underline{\mathbf{u}}(\underline{\mathbf{R}}',\omega)$ is an unknown function which has to be determined. Here, the Green's functions for the elastic half-space are chosen, where - considering the surface to be stress-free - the triadic stress-tensor function accordingly fulfills the boundary condition that

$$\underline{\mathbf{e}}_z\cdot\underline{\underline{\boldsymbol{\Sigma}}}^{half}\Big|_{z=0} = \underline{\underline{\mathbf{0}}}\,, \qquad (10)$$

so that

$$\underline{\mathbf{u}}(\underline{\mathbf{R}},\omega) = -\int\int_S \Big[\underline{\mathbf{e}}_z\cdot\underline{\underline{\mathbf{T}}}(\underline{\mathbf{R}}',\omega)\Big]\cdot\underline{\underline{\mathbf{G}}}^{half}(\Delta\underline{\mathbf{R}},\omega)\,\mathrm{d}S' \qquad (11)$$

follows, where the dyadic Green's function for the half-space has accordingly been introduced.

From Ref. 7, where the far-field radiation of vibrating point sources in anisotropic media is considered, a far-field expression for $\underline{\underline{\mathbf{G}}}^{half}$ accounting for the bulk wave contributions can be inferred according to

$$\underline{\underline{\mathbf{G}}}^{half}_{far}(\Delta\underline{\mathbf{R}},\omega) = \sum_\alpha \underline{\mathbf{g}}_\alpha\Big(\hat{\underline{\mathbf{K}}}(\widehat{\Delta\underline{\mathbf{R}}})\Big)\,\hat{\underline{\mathbf{u}}}_\alpha\Big(\hat{\underline{\mathbf{K}}}(\widehat{\Delta\underline{\mathbf{R}}})\Big)\,\frac{\mathrm{e}^{\mathrm{j}\underline{\mathbf{K}}_\alpha(\widehat{\Delta\underline{\mathbf{R}}})\cdot\Delta\underline{\mathbf{R}}}}{4\pi\mid\Delta\underline{\mathbf{R}}\mid}\,, \qquad (12)$$

where $\hat{\underline{\mathbf{u}}}_\alpha$ and $\underline{\mathbf{K}}_\alpha = K_\alpha\hat{\underline{\mathbf{K}}}$ designate the (plane wave) polarization vector and the wave vector of wavetype α, respectively. The Cartesian components of vector $\underline{\mathbf{g}}_\alpha$ are the directivities for transversely (in x- or y-direction) and normally (in z-direction) acting point sources on the stress-free surface. $\underline{\mathbf{g}}_\alpha$ and $\hat{\underline{\mathbf{u}}}_\alpha$ - as well as the group velocity vector $\underline{\mathbf{c}}_\alpha$ - are functions of the wave propagation direction $\hat{\underline{\mathbf{K}}}$ that produces an energy contribution along the spatial direction $\widehat{\Delta\underline{\mathbf{R}}}$. An efficient numerical evaluation scheme for the $\hat{\underline{\mathbf{K}}}(\widehat{\Delta\underline{\mathbf{R}}})$-relationship has been described in Ref. 2. Using Eq. (12) and defining the surface traction

$$\underline{\mathbf{t}}(\underline{\mathbf{R}}',\omega) \equiv \underline{\mathbf{e}}_z\cdot\underline{\underline{\mathbf{T}}}(\underline{\mathbf{R}}',\omega)\,, \qquad (13)$$

Eq. (11) finally leads to

$$\underline{\mathbf{u}}(\underline{\mathbf{R}},\omega) \cong -\int\int_S \sum_\alpha\Big[\underline{\mathbf{t}}(\underline{\mathbf{R}}',\omega)\cdot\underline{\mathbf{g}}_\alpha\Big(\hat{\underline{\mathbf{K}}}(\widehat{\Delta\underline{\mathbf{R}}})\Big)\Big]\cdot\hat{\underline{\mathbf{u}}}_\alpha\Big(\hat{\underline{\mathbf{K}}}(\widehat{\Delta\underline{\mathbf{R}}})\Big)\,\frac{\mathrm{e}^{\mathrm{j}\omega|\underline{\mathbf{R}}-\underline{\mathbf{R}}'|/c_\alpha(\widehat{\Delta\underline{\mathbf{R}}})}}{4\pi\mid\Delta\underline{\mathbf{R}}\mid}\mathrm{d}S', \qquad (14)$$

which is valid in the far-field of the point source, and which can be appplied to model transducer generated bulk wave fields in isotropic and anisotropic media. To circumvent the intricate the determination of $\underline{\mathbf{g}}_\alpha$ using Green's function, a method based on the reciprocity theorem is applied [8].

Assuming a traction whose magnitude is zero outside the transducer aperture and unity

within, the integration in Eq. (14) has to be performed over the transducer aperture. Numerical integration on the basis of an equally spaced rectangular grid can be applied for planar surfaces, with grid points separated at a distance of less than half a wavelength to fulfil the sampling theorem. For curved - e.g. cylindrical or spherical - surfaces a respective projection of a planar grid onto the curved surfaces is applied. If multiple element transducers are considered, the aperture is accordingly structured with tractions of zero or unity magnitude, respectively, where also additional phase delays can be introduced.

The results obtained for continuous wave displacement fields using this computational scheme are valid even in the near-field of the beam [2]. On the basis of Eq. (14), an efficient far-field approximation has been derived in [9], which is particularly useful in view of low calculation times.

In order to determine transducer beam fields for broadband input signals, a straight-forward computational approach for modeling of transient signals is applied, where the harmonic (cw) solution is calculated at many frequencies and then numerically Fourier transform this data into the time domain. In this approach, a function for the frequency spectrum of the transducer input signal has to be selected, e.g. to properly model an experimental input signal.

In modeling the insonification into a component using immersion technique, the evaluation of Eq. (14) is performed accordingly. The particle displacement is calculated at the interface grid points and used as the prescribed displacement distribution at this interface. Taking into account the respective boundary conditions, this distribution is then propagated from the interface into the material as described above. The same principle holds for defects and other disconituities with consideration of the appropriate point source directivities. Based on Kirchhoff's theory, this has been presented previously in Ref 10.

Gaussian Beam Superposition

To simulate the propagation of transducer generated wave fields, a procedure used to get a series solution to a boundary value problem can be applied [11]. Starting with the equation of motion ($\underline{\mathbf{f}} = \underline{\mathbf{0}}$), a Gaussian solution used as a base function is established, then the relevant boundary conditions are expressed in terms of a set of base functions.

For anisotropic materials, such Gaussian base functions have been given in [3]. The complete field solution is written as a superposition of these functions with different parameters U_n and M_n according to

$$\begin{aligned} \underline{\mathbf{u}}_\alpha(\underline{\mathbf{R}},\omega) &= \sum_{n=1}^{N} U_n\, \underline{\hat{\mathbf{u}}}_\alpha \exp[\mathrm{j}\underline{\mathbf{K}}_\alpha \cdot \underline{\mathbf{R}}] \cdot \mathcal{A}_{\alpha,n} \cdot \qquad (15) \\ &\cdot \exp\left[\frac{\mathrm{j}\omega}{2(\underline{\mathbf{c}}_\alpha \cdot \underline{\hat{\mathbf{K}}})}\, \underline{\mathcal{C}}_\alpha \cdot \underline{\underline{\mathbf{M}}}_{\alpha,n}(\underline{\mathbf{R}}) \cdot \underline{\mathcal{C}}_\alpha\right], \end{aligned}$$

where $\underline{\mathcal{C}}_\alpha \equiv (\underline{\mathbf{c}}_\alpha \cdot \underline{\hat{\mathbf{K}}})\underline{\mathbf{R}} - (\underline{\mathbf{R}} \cdot \underline{\hat{\mathbf{K}}})\underline{\mathbf{c}}_\alpha$, N is the number of GB-functions required. In this representation, $\mathcal{A}_{\alpha,n}$ accounts for the geometrical spreading as the beam moves through the medium, while the matrix $\underline{\underline{\mathbf{M}}}_{\alpha,n}$ determines the Gaussian shape of the beam [3]. Both quantities depend on M_n, which are the complex beam waist parameters of the GB-functions; further, U_n are the (complex) amplitudes. Equation (15) has to satisfy the boundary conditions by properly determining the coefficients M_n and U_n of the base functions. In the following, a ten-term GB-solution is applied using coefficients given in [11].

In the derivation of the Gaussian beam series solution, harmonic time dependence was assumed. However, in practical application generally beams of finite pulse length are of interest; these pulsed solutions are obained as already described in the previous section.

Application to Transducer Optimization

For industrial components of arbitrary shape, the transducer fields strongly depend on the material or interface curvatures and the coupling conditions. Thus, simulation of transducer sound fields is most useful for evaluating measured signals and for designing transducers which are optimized for the respective set-up. Due to the large number of transducer parameters and their complex influence on the sound field, experimental work can thus be significantly reduced, which is useful for both single-element and multiple element transducers.

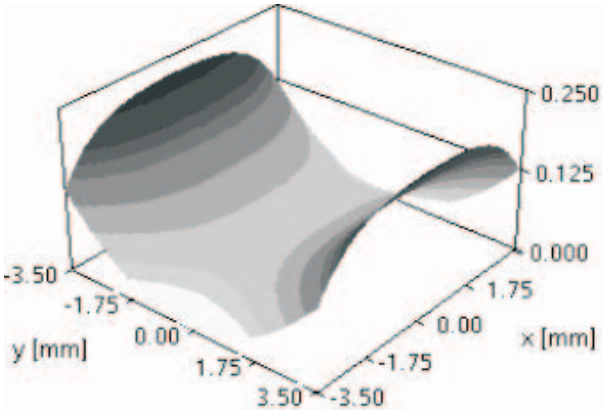

Figure 1 : Geometry of the optimized piezoelement applied to focus to a depth of 6 mm (expanded scale along z-axis).

Immersion Probe for Cylindrical Component Inspection

The component to be inspected is a steel pipe with an inner diameter of 34 mm and a wall thickness of 20 mm. Using immersion technique, the pipe is assumed to be tested for defects from the interior, with high sensitivity in a range from 4 mm to 8 mm depth. Usually, the inspection of such components is performed using socalled bifocal transducers. Such line-focusing probes exhibit beam fields which are focused in the axial plane, but diverging in the radial plane, with an additional focal spot being generated due to the component's curvature. To improve the inspection performance, a transducer has been elaborated, which - operated at 10 MHz frequency - three-dimensionally focusses the beam field to a depth of 6 mm. In the optimzation, both frequency and the piezoelement dimensions have been varied, while a fixed immersion distance of 15 mm has been assumed according to the inner pipe diameter. Details on the optimization procedure can be found in Ref. 12.

As shown in Fig. 1, the calculated shape of the rectangular piezoelement of 7 x 7 mm^2 is characterized by a convex curvature of 80 mm radius in the radial plane, and a concave curvature in the axial plane (radius 40 mm). The beam field calculated for this transducer configuration is shown in Fig. 2. The desired coverage of the depth range from 4 mm to 8 mm is achieved within an amplitude range between 0 dB and -6 dB as indicated. The amplitude continuously

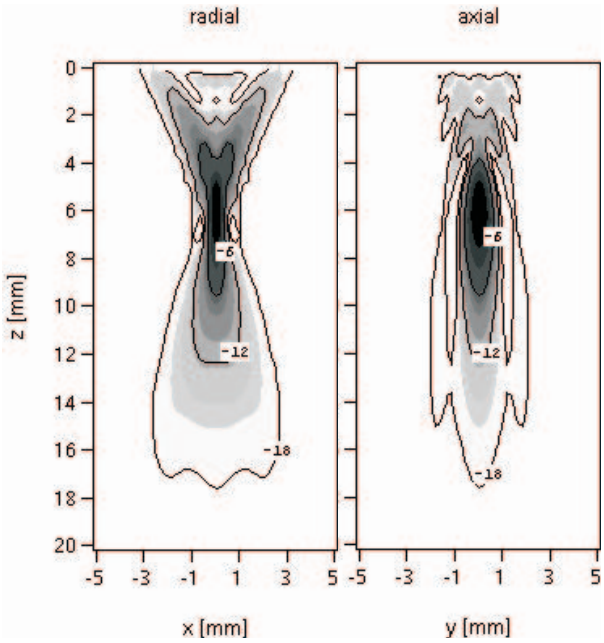

Figure 2 : Beam field representations for the optimized transducer in the radial (left) and axial (right) plane (frequency 10 MHz, immersion distance 15 mm).

decreases, at a depth of 15 mm it is still approximately -15 dB with respect to the absolute maximum value. For the optimized probe, the absolute maximum of the beam field is approximately 5 times as high as compared to the absolute maximum produced by a commercial line-focusing transducer of similar dimensions [12].

Phased Array on Composite Material

The anisotropic elastic behaviour of modern structural materials like composites and the resulting wave propagation characteristics lead to considerable difficulties in applying conventional ultrasonic inspection procedures. However, the effects of beam field skewing and distortion can be considerably compensated by proper focusing and steering of array transducer fields.

As an example, the beam fields generated by a conventional angle-beam array transducer have been evaluated and optimized for a layered [0_3/90]-composite material. The elastic characteristics of this material are described in Ref. 13. The 2 MHz-probe - applied to generate (quasi-) longitudinal waves - consists of a rectangular transducer (16x8 mm^2) mounted on a perspex wegde. The wedge angle is 19.6^o resulting in an

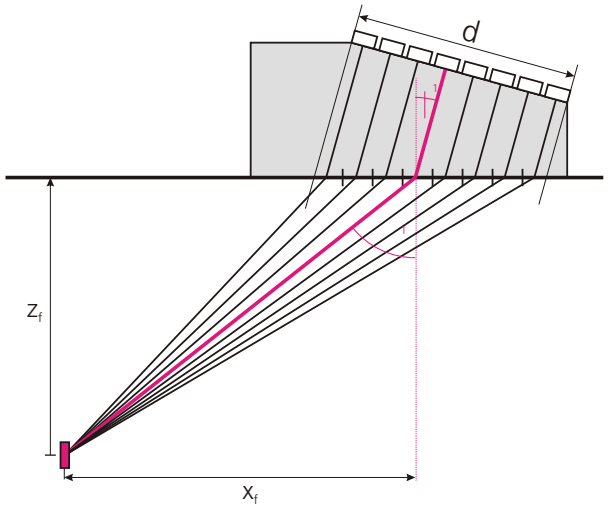

Figure 3 : Schematic sketch of a conventional angle-beam array transducer. Beam focusing to the point (x_f, z_f) is accomplished by delay time calculation using the anisotropic material's elastic properties.

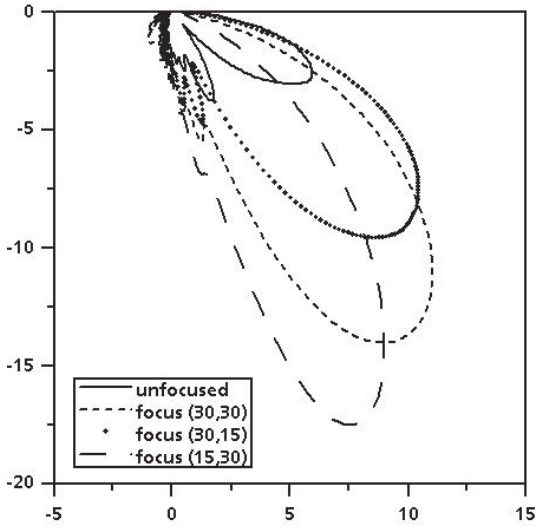

Figure 4 : Polar plots of the beam field directivity patterns calculated at a distance of $r = 40$ mm for various focal modes at indicated in the legend (composite's layers parallel to the surface).

insonification angle of 45° in ferritic steel. In calculating the delay times for the 16 elements, the directionally dependent ultrasonic velocities have been taken into consideration. As schematically shown in Fig. 3, the delay times are determined for each element in order to focus the generated beam to a focal point with coordinates (x_f, z_f) in the plane of insonification.

Figure 4 displays polar plots of the probe's directivity patterns - calculated at a distance of $r = 40$ mm for various focal modes. The solid line represents the directivities without time-delayed excitation of the elements. As expected, the insonification angle is different from 45°, which is obtained in ferritic steel. However, point focusing allows to direct the beam field to various angles and even improve the field amplitudes, as represented by the dashed curves in Fig. 4. Thus, the difficulties usually experienced in inspecting anisotropic materials, i.e. beam skewing and distortion effects, can be considerably minimized.

Application to Inspection Simulation

The ultrasonic signals picked up by a transducer in a - as an example - pulse-echo (PE)inspection experiment are determined in the following way. First, the transducer-generated displacement distribution is calculated at the position of the scatterer using Eq. (14), then the scattered wave field is determined as described in detail in [10]. The (time-domain) signal detected by the transducer is finally determined using Auld's reciprocity theorem which exploits the displacement and traction at the scatterer's position in presence and absence of the scatterer, respectively [14]. A similar procedure can be applied on the basis of Eq. (15).

The far-field expressions derived in [9] for planar vibrating sources can be used to perform approximate calculations. Thus, a simple expression can be formulated e.g. for the amplitude dynamic curves (ADC) measured in a pulse-echo inspection experiment. Although the influence of the traction-free material surface on the transducer radiation characteristics as well as the particular boundary conditions at the scatterer are neglected in using this relationship, the results compare well with those obtained on the basis of Eq. (14) [9].

Amplitude dynamic curves in composites

Two unidirectionally carbon-fiber reinforced composite specimens with fibers being orientated at 15° (No. 1) and 75° (No. 2) to the surface, respectively, have been examined. These specimens were supplied with a number of 3 mm and 5 mm flat-bottom holes (FBH) at various depths. The pulse-echo experiments have

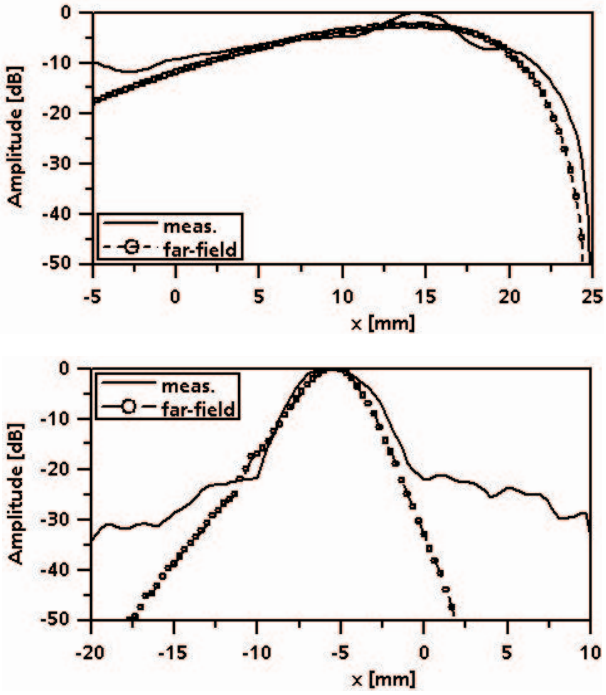

Figure 5 : Simulated and measured pulse-echo amplitude dynamic curves for 5 mm flat-bottomed holes in a unidirectional composite. The fibers are aligned at an angle of 15° (top, defect depth 15 mm) and 75° (bottom, defect depth 30 mm) to the surface. Note the different scan paths ($x = 0$ mm marks the lateral defect position).

been performed with a piezoelectric normal-transducer of 2.25 MHz frequency and 6.3 mm in diameter (Krautkrämer MSW-QC 2,25), generating (quasi-) longitudinal waves. Further details on the measurements can be found in [15]. For these inspection parameters, ADCs have been simulated using the far-field relationships given in Ref. 9. As an example, Figure 5 shows the results obtained for 5 mm FBHs, which were located in a depth of 15 mm in specimen No. 1 and in a depth of 30 mm in specimen No. 2. In the latter case, the measured ADC does not drop below -30 dB, due to the experimental noise level. In these results, the effects of wave field spreading and skewing are more or less apparent. Good agreement between the simulated and the measured ADCs is obtained, with differences in the order of about 2 to 3 dB.

Inspection of Austenitic Welds

Simulation with respect to the optimization

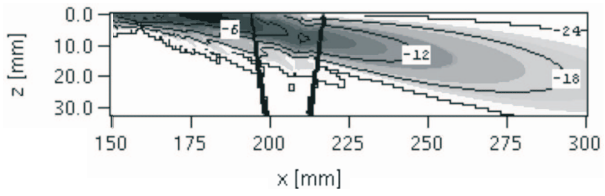

Figure 6 : Beam field of an 80°-angle beam transducer insonifying a V-weld. The probe's index point is located at 160 mm, while the weld is located at approx. 200 mm. The logarithmic scaling ranges down to - 24 dB.

of ultrasonic inspections is in the following exemplified for a V-weld in an austenitic plate with a surface connected crack-like defect. Micrographs have been used to establish a model to describe the inhomogeneous weld microstructure [16]. The weld is divided into several layers, each of them being characterized by a grain orientation according to this model and exhibiting transversely isotropic elastic behaviour. First, the wave fields passing through the weld, as generated by commercial ultrasonic angle beam transducers, have been determined applying the GB-method, details of the modeling procedure can be found in [4]. The calculations reveal that for a standard inspection procedure using longitudinal waves at 45°, 60° or 70° incidence the desired inspection volume may be properly covered. However, operating the transducers in pulse-echo mode, due to the anisotropy of the weld, the ultrasonic waves reflected at the defect - positioned at the weld flank - travel at different paths and can thus not be detected.
A variation of the angle of incidence reveals, that an optimal detection will occur at 80°, in this case the defect is hit perpendicularly. The respective beam field for a circular transducer (frequency 4 MHz, diameter 9 mm) mounted on a wedge is exemplarily shown in Fig. 6. The bending of the beam field due to the weld's microstructure occurs mainly in the weld's mid-region. Quantitative information on the defect signal is gained by calculating RF-ultrasonic signals usually acquired in a pulse-echo experiment. The simulated RF-data for the optimized angle of incidence, where only the specularly reflected longitudinal wave has been taken into consideration, can be further evaluated. Con-

sidering the probe coordinates and the ultrasonic velocities using Synthetic Aperture Focusing Techniques, the efficiency of the optimized inspection set-up versus the standard type inspection is revealed [16].

Summary

Analytical approaches to model ultrasonic nondestructive evaluation in general allow for reasonable calculation times. These models can be employed to consider the various wave phenomena separately, which is desirable from the practical point of view. Since approximations are applied, the approaches have to be selected according to the respective problem of interest. The presented methods are three-dimensional approaches and have been verified in comparison with experimental results previously. On standard PCs, the calculation times for the GB solution are in the order of seconds. For frequencies in the range from 0.5 to 5 MHz, which is usually of interest in ultrasonic NDT, point source superposition provides simulation results within minutes, while calculations based on the far-field approximation can be also performed within seconds. The reviewed simulation methods can be efficiently employed to clearify wave propagation effects and to optimize transducers as well as inspection procedures.

References

[1] M. Spies, "Transducer-modeling in general transversely isotropic media via point-source-synthesis. Theory," J. Nondestr. Eval., vol. 13, pp. 85-99, 1994

[2] M. Spies, "Semi-analytical elastic wave-field modeling applied to arbitrarily oriented orthotropic media," J. Acoust. Soc. Am., vol. 110, pp. 68-79, 2001

[3] M. Spies, "Transducer field modeling in anisotropic media by superposition of Gaussian base functions," J. Acoust. Soc. Am., vol. 105, pp. 633-638, 1999

[4] M. Spies, "Modeling of transducer fields in inhomogeneous anisotropic materials using Gaussian beam superposition," NDT&E International, vol. 33, pp. 155-162, 2000

[5] Y.H. Pao, V. Varatharajulu, "Huygens' Principle, Radiation Conditions and Integral Formulas for the Scattering of Elastic Waves," J. Acoust. Soc. Am., vol. 59, pp. 1361-1371, 1976

[6] Q.C. Guo, J.D. Achenbach, "Radiation of Ultrasound into an Anisotropic Solid," Ultrasonics, vol. 33, pp. 449-456, 1995

[7] K. Wu, P.B. Nagy, L. Adler, "Far-field radiation of a vibrating point source in anisotropic media," J. Nondestr. Eval., vol. 10, pp. 71-78, 1991

[8] K. Wu, P.B. Nagy, L. Adler, "Far Field Radiation of a Point Source on the Free Surface of Semi-Infinite Anisotropic Solids," in Review of Progress in Quantitative NDE, eds. D.O. Thompson and D.E. Chimenti, Plenum Press, New York, 1990, vol. 9A, pp. 149-156

[9] M. Spies, "Quantitative evaluation of defects in anisotropic media using the far-field radiation characteristics of vibrating sources," in Review of Progress in QNDE, eds. D.O. Thompson and D.E. Chimenti, Plenum Press, New York,2002, vol. 21, pp. 107-114

[10] M. Spies, "Kirchhoff evaluation of scattered elastic wavefields in anisotropic media," J. Acoust. Soc. Am., vol. 107, pp. 2755-2759, 2000

[11] J.J. Wen, M.A. Breazeale, "A diffraction beam field expressed as the superposition of Gaussian beams," J. Acoust. Soc. Am., vol. 83, pp. 1752-1756, 1988

[12]M. Spies, "Efficient Optimization of Single and Multiple Element Transducers for the Inspection of Complex-Shaped Components," NDT&E International, submitted for publication

[13] B. Hosten, M. Deschamps, B.R. Tittmann, "Inhomogeneous wave generation and propagation in lossy anisotropic solids," J. Acoust. Soc. Am., vol. 82, pp. 1763-1770, 1987

[14] B.A. Auld, "General electromechanical reciprocity relations applied to the calculation of elastic wave scattering coefficients," Wave Motion, vol. 1, pp. 3-10, 1979

[15] M. Spies, W. Jager, "Synthetic aperture focusing for defect reconstruction in anisotropic media," Ultrasonics, vol. 41, pp. 125-131, 2003

[16] M. Spies, V. Schmitz, W. Müller, "A simulation-based methodology to optimize nondestructive inspection of austenitic welds," in Mathematical Modelling of Weld Phenomena 7, ed. H. Cerjak, Maney Publishing, London, to be published